7-11-2011

Evidence of the $2s2\,p(^1P)$ doubly excited state in the harmonic generation spectrum of helium

Jean Marcel Ngoko Djiokap
University of Nebraska-Lincoln, marcelngoko@unl.edu

Anthony F. Starace
University of Nebraska-Lincoln, astarace1@unl.edu

Evidence of the $2s2p(^1P)$ doubly excited state in the harmonic generation spectrum of helium

J. M. Ngoko Djiokap and Anthony F. Starace
Department of Physics and Astronomy, The University of Nebraska, Lincoln, Nebraska 68588-0299, USA
(Received 5 April 2011; published 11 July 2011)

By solving the two-active-electron time-dependent Schrödinger equation in an intense, ultrashort laser field, we investigate evidence of electron correlations in the high-order harmonic generation spectrum of helium. As the frequency of the driving laser pulse varies from 4.6 to 6.6 eV, the 13th, 11th, and 9th harmonics sequentially become resonant with the transition between the ground state and the isolated $2s2p(^1P)$ autoionizing state of helium, which dramatically enhances these harmonics and changes their profiles. When each of the 9th and 13th harmonics are in resonance with this autoionizing state, there is also a low-order multiphoton resonance with a Rydberg state, resulting in a particularly large enhancement of these harmonics relative to neighboring harmonics. When the 11th harmonic is in resonance with the $2s2p(^1P)$ autoionizing state, the 13th harmonic is simultaneously in resonance with numerous higher-energy autoionizing states, resulting in a competition between these two harmonics for intensity. These results demonstrate that even electron correlations occurring over a narrow energy interval can have a significant effect on strong-field processes such as harmonic generation.

DOI: 10.1103/PhysRevA.84.013404 PACS number(s): 32.80.Rm, 42.65.Ky, 32.80.Zb

I. INTRODUCTION

High-order harmonic generation (HHG) has been a key focus of strong-field physics for more than two decades owing to both its intrinsic interest and its many important applications, such as, e.g., for producing attosecond pulses, for producing high-energy harmonics in the important water-window region, and for imaging atomic, molecular, and other target systems [1–3]. In the important low-frequency tunneling regime, defined by a Keldysh parameter $\gamma \equiv \sqrt{I_p/2U_p} \ll 1$ (where I_p is the binding energy of the active electron and U_p is its ponderomotive potential energy in the laser field), the three-step scenario [4,5] (i.e., ionization by tunneling, laser-driven electron motion away from and back to the target ion, and recombination of the electron with harmonic emission) has proved to be an invaluable guide for understanding HHG [6]. More recent is the idea that (in the tunneling regime) the HHG rate near the cutoff of the HHG plateau is proportional to the field-free photorecombination cross section [7–11]. Explicit analytic factorized formulas for the HHG rate (with each of the three factors corresponding precisely to the three steps of the three-step scenario) have been derived [12–15], with the factor for the third step being the field-free photorecombination cross section. Whereas in most theoretical works in strong-field physics the single active electron approximation is made, the proportionality of the HHG rate to the field-free photorecombination cross section led to the prediction of strong multielectron effects on the HHG rate for the rare gases [13] that have now been confirmed experimentally [16]. Resonance effects in earlier HHG experiments on transition metal plasmas [17–19] have also recently been explained as stemming from multielectron effects on the field-free photorecombination cross section [20]. It should be emphasized that in the multiphoton regime, defined by $\gamma \equiv \sqrt{I_p/2U_p} > 1$, the three-step scenario is not applicable, and the role of multielectron correlations on HHG in this regime remains an open question.

The HHG spectrum of helium has been of interest in strong-field physics for a long time. In particular, it was the element in which experimentalists first observed harmonics in the water-window region [21,22] and among those for which harmonics with significant intensities in this soft x-ray region have recently been obtained [23]. Theoretically, the helium atom, which is the simplest and most fundamental many-electron atom, has long served as a test bed for *ab initio* treatments of electron correlations in atomic processes in general, including intense laser-atom interaction processes such as HHG. Lambropoulos *et al.* [24] reviewed investigations of intense laser interactions with two-electron systems up to around 1997. Since that review, the number of theoretical investigations of intense laser-atom processes involving He has increased greatly, not only for HHG [25–34] but also for multiphoton ionization processes [25,35–42] and, especially, for two-photon double-ionization processes [43–60].

The role of autoionizing states on intense laser-atom processes (representing a particular kind of many-electron correlation) has also been of interest in strong-field physics for a long time (see, e.g., Ref. [61]). Moreover, theoretical interest in this problem has grown recently [62–72], with nearly all of these investigations focused on the time evolution of an autoionization process. A few of these theoretical investigations concern laser ionization of the He atom [63,66,70]. Two present general models for the role of autoionization in HHG in the tunneling regime [68,69]. Among recent theoretical works on HHG in He [25–34], most focus on the general role of electron correlation on the HHG spectrum (e.g., as compared to results of single-active-electron calculations) rather than on the role of particular autoionizing states. The work of Guan *et al.* [33] does note the influence of a group of particular autoionizing states on the HHG spectrum of He. In general, studies of the He HHG spectrum have been carried out for particular driving laser frequencies, with the most detailed theoretical calculations involving higher frequencies (in part, in order to reduce the number of angular momentum components involved). Recently, an experiment on the harmonic supercontinuum spectrum of He as a function of photon frequency observed a "prominent peak" in the spectrum at a photon energy of ≈60 eV, which the authors attributed to the He $2s2p(^1P)$ autoionization state [73].

The focus of this paper is on identifying the influence of the well-isolated, doubly excited autoionizing state $2s2p(^1P)$ on the harmonic generation spectrum of helium. The He atom is chosen because it has only two electrons, so that we are able to treat all electron correlation effects exactly by solving the full-dimensional, two-electron Schrödinger equation. Our numerical methods are similar to those employed to treat laser detachment of the lithium negative ion in Refs. [74,75], modified appropriately, of course, to describe laser-driven, harmonic generation by the helium atom. In order to reduce the number of angular momentum components necessary to achieve converged results, we focus on photon energies in the range 4.6 eV $\leqslant \hbar\omega_L \leqslant$ 6.6 eV, within which lie the fundamental frequency of the KrF laser and the 3rd, 4th, and 5th harmonics of the tunable Ti:sapphire laser. By presenting results as a function of laser frequency, the effects of the autoionization resonance become clear. Finally, in order to reduce effects of laser intensity, we focus in this paper on the multiphoton regime.

The organization of this paper is as follows: In Sec. II we describe the essentials of our theoretical approach. In Sec. III, we present our numerical results and analyses. Finally, in Sec. IV, we briefly summarize our results and draw some conclusions. Note that we employ atomic units ($e = \hbar = m = 1, c = 1/\alpha$) throughout this paper, unless otherwise stated.

II. THEORETICAL APPROACH

We describe here our theoretical approach and numerical methods. Our program for solving the two-electron time-dependent Schrödinger equation (TDSE) is modified from that used in Refs. [74,75] to treat short-pulse laser detachment of the negative ion of lithium, which was reduced to a two-electron problem by describing the inner $1s$-subshell electrons and the nucleus by an effective potential. We describe first our procedure for calculating field-free states of the He atom. Then we present our approach for solving the two-electron TDSE for the He atom interacting with a laser pulse. Finally, we describe our calculation of the electric dipole amplitude in the velocity gauge, from which we obtain HHG rates.

A. Atomic structure calculation

The helium atom is treated as a two-active electron system in which the two-electron states are expanded in terms of one-electron basis orbitals chosen to be the eigenstates of the He^+ ion, i.e., each one-electron basis orbital describes an electron in the Coulomb potential $V(r) = -Z/r$ describing the He^{++} core (with nuclear charge $Z = 2$). As in Refs. [74–76], the radial function describing each one-electron basis orbital (with angular momentum l, radial quantum number n, and energy ϵ_n) is given by

$$\left[-\frac{1}{2}\frac{d^2}{dr^2} + \frac{l(l+1)}{2r^2} - \frac{Z}{r}\right] R_{nl}(r) = \epsilon_n R_{nl}(r). \tag{1}$$

The nonrelativistic Hamiltonian for the He atom is

$$H = -\frac{1}{2}\Delta_1^2 - \frac{1}{2}\Delta_2^2 - \frac{Z}{r_1} - \frac{Z}{r_2} + \frac{1}{|\vec{r}_1 - \vec{r}_2|}, \tag{2}$$

where

$$\Delta_1^2 = \frac{d^2}{dr_1^2} - \frac{l(l+1)}{r_1^2}, \quad \Delta_2^2 = \frac{d^2}{dr_2^2} - \frac{l'(l'+1)}{r_2^2}, \tag{3}$$

and $\vec{r}_1$ and $\vec{r}_2$ are the spatial coordinates of the two electrons. The following multipole expansion of the electron-electron electrostatic potential $r_{12}^{-1} \equiv |\vec{r}_1 - \vec{r}_2|^{-1}$ is used:

$$\frac{1}{r_{12}} = 4\pi \sum_{k=0}^{\infty} \sum_{q=-k}^{k} \frac{1}{2k+1} \frac{r_<^k}{r_>^{k+1}} Y_{kq}^*(\hat{r}_<) Y_{kq}(\hat{r}_>), \tag{4}$$

where $Y_{kq}(\hat{r})$ denotes a spherical harmonic.

A two-electron helium eigenfunction Ψ of energy E is a solution of the following equation:

$$H\Psi = E\Psi. \tag{5}$$

For a given total angular momentum L and projection M, we use the following configuration interaction (CI) expansion of the solution of Eq. (5):

$$\Psi^{LM}(\vec{r}_1,\vec{r}_2) = \sum_{l,l'} \sum_{n,n'} \psi_{nn'}^{ll'LM} \mathcal{A} F_{nn'}^{ll'LM}(\vec{r}_1,\vec{r}_2), \tag{6}$$

where $\psi_{nn'}^{ll'LM}$ is the expansion coefficient and

$$F_{nn'}^{ll'LM}(\vec{r}_1,\vec{r}_2) = \frac{R_{nl}(r_1)}{r_1} \Lambda_{ll'}^{LM}(\hat{r}_1,\hat{r}_2) \frac{R_{n'l'}(r_2)}{r_2}. \tag{7}$$

The normalized antisymmetrization operator $\mathcal{A} \equiv (1 + \varepsilon P_{12})/\sqrt{2}$ in Eq. (6) is such that $\varepsilon = +1$ (-1) for singlet (triplet) states and the operator P_{12} exchanges the parameters (nl) and $(n'l')$ in order to properly account for the indistinguishability of the two electrons. Thus $\mathcal{A}$ projects onto either singlet or triplet states to ensure the symmetry or the antisymmetry of the spatial wave function, as required by the Pauli principle. The angular part of the expansion in Eq. (6) is expressed in Eq. (7) in terms of the bipolar harmonics,

$$\Lambda_{ll'}^{LM}(\hat{r}_1,\hat{r}_2) = \sum_{m,m'} \langle lm,l'm'|LM\rangle Y_{l,m}(\hat{r}_1) Y_{l',m'}(\hat{r}_2), \tag{8}$$

which couple the two individual electron angular momenta l and l' in the LS-coupling scheme, where $\langle lm,l'm'|LM\rangle$ is a Clebsch-Gordan coefficient. In this paper we only consider the case of linearly polarized light and assume that electric dipole selection rules hold. Consequently, since the initial state of He in LS coupling is an even-parity ^1S state, the LS-coupled individual angular momenta of the electrons in laser-excited states must satisfy $(-1)^L = (-1)^{l+l'}$.

The radial wave functions R_{nl} are obtained (for both $\epsilon_n \leqslant 0$ and $\epsilon_n > 0$) by solving Eq. (1) in a radial box of size $r = r_0$, with boundary conditions $R_{nl}(r_0) = 0$ [74,75]. Note that both bound and continuum one-electron orbitals are included in the basis expansion, so that the resulting basis set is complete (except for truncation). In Eq. (6), the expansion coefficients $\psi_{nn'}^{ll'LM}$ are obtained by requiring that the expansion in Eq. (6) is a solution of the time-independent Schrödinger equation (5). By performing a single diagonalization of the atomic Hamiltonian for each value of the total angular momentum L, we obtain discrete eigenenergies corresponding to bound states and to pseudostates representing the continuum.

B. Time-dependent calculation

We now consider the interaction between the atom and the laser field. Within the electric dipole approximation, the TDSE in the velocity gauge is

$$i\frac{\partial}{\partial t}\Psi_V(\vec{r}_1,\vec{r}_2,t) = [H + D_V(t)]\Psi_V(\vec{r}_1,\vec{r}_2,t), \tag{9}$$

where $D_V(t) = \vec{A}(t)\cdot(\vec{p}_1 + \vec{p}_2)$. The vector potential and the electric field, polarized along the z axis, are defined in the interval $-T/2 \leqslant t \leqslant T/2$ as

$$\vec{A}(t) = A_0 f(t)\sin(\omega_L t + \phi)\vec{e}_z, \vec{E}(t) = -\frac{\partial}{\partial t}\vec{A}(t), \tag{10}$$

where ω_L is the laser photon energy, ϕ is the so-called carrier-envelope phase (CEP), and T is the total pulse duration. The peak intensity of the laser field is given by $I = E_0^2$, where $E_0 \equiv A_0\omega_L$. The pulse envelope $f(t)$ in our calculations either has a squared cosine form, i.e.,

$$f(t) = \begin{cases} \cos^2(\pi t/T), |t| \leqslant T/2 \\ 0, \quad \text{otherwise}, \end{cases} \tag{11}$$

or a trapezoidal (flat-top) profile [25,63]. In the latter case, the laser pulse is ramped on and off over eight optical cycles, with a total duration of $N_c = 30$ optical cycles. Owing to the large number of optical cycles in our laser pulse, CEP effects are negligible. We note that most of our results are obtained for the case of a trapezoidal pulse. Toma *et al.* [77] have found experimentally that resonance effects in HHG that may not be visible for a Gaussian-shaped focus could be observed for a spatially shaped flat-top focus, which we model in our calculations by a trapezoidal laser pulse. We do compare in one case the single-atom HHG spectrum obtained for a Gaussian pulse with that for a trapezoidal pulse.

The solution of the TDSE (9) in a box uses the following time-dependent CI expansion of the wave function:

$$\Psi_V(\vec{r}_1,\vec{r}_2,t) = \sum_{L,M}\sum_{ll'}\sum_{nn'}\Upsilon_{nn'}^{ll'LM}(t)\mathcal{A}F_{nn'}^{ll'LM}(\vec{r}_1,\vec{r}_2), \tag{12}$$

where $\Upsilon_{nn'}^{ll'LM}(t)$ is the time-dependent expansion coefficient. Since in our calculations we assume (i) LS coupling, (ii) a linearly polarized laser field, and (iii) that the initial state of helium is ^1S, we can set $M = 0$ in the expansion (12). The solution of the TDSE (9) can be carried out as in Sec. II of Ref. [75]. In brief, by projecting Eq. (9) on the basis functions $\mathcal{A}F_{nn'}^{ll'LM}(\vec{r}_1,\vec{r}_2)$ and integrating over the spatial coordinates of both electrons, the TDSE reduces to a set of coupled first-order differential equations, which may be expressed in matrix form as follows:

$$i\frac{\partial}{\partial t}\Upsilon(t) = [\mathbf{H} - iA(t)\mathbf{D}]\Upsilon(t). \tag{13}$$

Owing to the stiffness of the time propagation, it is best to transform Eq. (13) from the original basis to the field-free, two-electron eigenfunction basis. This can be done by using the orthogonal matrix $\mathbf{P}$ of eigenvectors of $\mathbf{H}$ and its transpose $\mathbf{P}^t$, where $\mathbf{H}$ is a real matrix associated with the field-free atomic Hamiltonian (2). If $\mathbf{D}$ represents the real matrix associated with the projection of the electric dipole operator on the laser polarization direction, solving the TDSE is equivalent to solving

$$i\frac{\partial}{\partial t}\Phi(t) = [\mathbf{h} - iA(t)\mathbf{W}]\Phi(t), \tag{14}$$

where $\mathbf{h} = \mathbf{P}^t\mathbf{H}\mathbf{P}$ is the diagonal matrix of $\mathbf{H}$ and $\mathbf{W} = \mathbf{P}^t\mathbf{D}\mathbf{P}$ is comprised of the dipole matrix elements coupling various eigenvalues of $\mathbf{H}$. Note that the matrices $\mathbf{W}$ and $\mathbf{D}$ have the same structure, which is governed by electric dipole selection rules. The solution $\Phi(t)$ of Eq. (14) in the atomic (eigenstate) basis represents a linear superposition of two-electron eigenstates of $\mathbf{H}$, i.e.,

$$\Phi(t) = \sum_{n,L} C_{n,L}(t)\Phi_{n,L}, \tag{15}$$

where $\Phi_{n,L}$ is a two-electron eigenstate of energy E_n and $C_{n,L}(t)$ is its probability amplitude. Note that $\Upsilon(t)$ can be easily deduced from $\Phi(t)$ by the matrix vector product $\Upsilon(t) = \mathbf{P}\Phi(t)$. Starting from the field-free ground state of helium, we solve Eq. (14) using an embedded Runge-Kutta method of order 5. The norm of the wave packet (which is the density of the two-electron atomic states) is an important parameter for controlling the propagation. For all input parameters used in this paper, we have confirmed that this density is conserved.

C. HHG power spectrum

Our calculations are based on the following considerations. First, owing to gauge invariance, one can calculate the HHG power spectrum using the induced dipole length, dipole velocity, or dipole acceleration forms of the electric dipole operator. However, working in either the length gauge or the acceleration gauge requires accurate two-electron wave packets at either large or small radial coordinates, respectively, whereas the velocity gauge requires accurate wave packets at intermediate radial coordinates. Second, we employ a moderate laser peak intensity of 10^{14} W/cm^2, which is well below the saturation intensity [78], so that even high harmonics are due to He rather than He^+. Finally, we have selected a range of frequencies such that the ponderomotive energy and the quiver amplitude never exceed 0.7 eV and 2.0 a.u., respectively. For these reasons, we have found that using the dipole velocity form of the electric dipole interaction operator and a radial box size of $r_0 = 30$ a.u. allows us to obtain converged results for the power spectrum of HHG. The expectation value of the dipole velocity operator can be obtained either in the original basis, i.e.,

$$d_V(t) = \langle\Psi_V(\vec{r}_1,\vec{r}_2,t)| - i\frac{\partial}{\partial z_1} - i\frac{\partial}{\partial z_2}|\Psi_V(\vec{r}_1,\vec{r}_2,t)\rangle, \tag{16}$$

or in the eigenstate basis, i.e.,

$$d_V(t) = -i\langle\Phi(t)|\mathbf{W}|\Phi(t)\rangle. \tag{17}$$

We calculate the time-dependent dipole velocity amplitude using Eq. (17) and then calculate the HHG power spectrum in terms of its Fourier transform:

$$d(\omega) = \frac{i}{\omega T}\int_{-T}^{T} dt e^{-i\omega t}d_V(t), \quad \mathcal{P}(\omega_L;\omega) = |d(\omega)|^2. \tag{18}$$

III. NUMERICAL RESULTS

In this section we present first details of our numerical calculations for both the He atom eigenstates in the absence of a laser and for HHG in the presence of a laser field. Our purpose is to demonstrate the accuracy of our numerical solutions of the time-independent and time-dependent two-electron Schrödinger equation. We then present our results, which focus on the role of the He $2s2p(^1P)$ autoionizing state on the 9th, 11th, and 13th harmonics as a function of driving laser frequency ω_L.

A. Details of our calculational procedures

In our calculations we use a basis of He^+ one-electron radial functions $R_{nl}(r)$ [cf. Eq. (1)], where $0 \leqslant l \leqslant 5$ and, for a given value of l, $l+1 \leqslant n \leqslant l+30$. We employ six values of the total angular momentum L, where $0 \leqslant L \leqslant 5$, which has been found to be sufficient in HHG calculations for similar laser parameters by Guan *et al.* [33]. For each total angular momentum L, we use four pairs of one-electron angular momenta (l,l'), i.e., for a given L and a given value of l, where $0 \leqslant l \leqslant 5$, we chose l' according to the usual angular momentum and parity selection rules and, to avoid redundancy, $l \leqslant l'$. Finally, each one-electron radial coordinate is evaluated on a mesh having $N_{\rm mesh} = 2500$ points up to the maximum value $r_0 = 30$ a.u.

With such calculational parameters, in the absence of a laser field, we obtain a ground-state energy of $-2.895\,1719$ a.u. By decreasing the box size to $r_0 = 20$ a.u. and increasing the number of radial functions up to 70 for the lowest angular momentum pair (0,0), we obtain a ground-state energy of $-2.902\,168$ a.u., which compares well with the nonrelativistic result of Drake (see Table 11.5 of Ref. [79]), i.e., $-2.903\,724\,3770$ a.u. We have increased the size of our ground-state energy calculation simply to show that our programs are capable of obtaining highly accurate (nonrelativistic) energies. However, for all other calculations in this paper we have employed the more manageable size of basis specified in the prior paragraph.

The accuracy obtained by our numerical methods using the parameters specified above may be judged by our results for the absolute energies of the excited states of He. Our results for the singly excited states are given in Table I, where they are compared with those of Guan *et al.* [33] and Drake [79]. The agreement is good to four or five digits. Our results for the doubly excited states are given in Table II, where they are compared with those of Guan *et al.* [33], Drake [79], Scrinzi and Piraux [31], Ho [80], and Lindroth [81]. In almost all cases shown, the agreement is good to three digits. For future reference, in Fig. 1 we provide a diagram of the field-free singly and doubly excited states of He with excitation energies (in eV) above the ground state.

B. Considerations for observing autoionization states in He HHG

As may be seen from Table II, the odd-parity autoionizing state $2s2p(^1P)$ in our calculations is located at an energy of 59.91 eV above the even-parity ground state. (This excitation energy compares well with the experimental value of 60.0 ± 0.1 eV [82].) In addition, as shown in Table II, this autoionizing state has the virtue that it is reasonably isolated from other odd-parity doubly excited states. In order to probe this autoionizing state by means of HHG one must require that the driving laser frequency has a value such that an odd number N of laser photons is in resonance with this state, i.e., $\omega_L^{\rm res}(N) = E_{2s2p(^1P)}/N$. For driving laser frequencies in the range from 4.6 to 6.6 eV, one can thus achieve resonance with this autoionizing state by 9-, 11-, or 13-photon transitions, as shown in Table III. Also, we have highlighted in bold in Table III those harmonics of these three driving laser frequencies that are close to being in resonance with some of the singly excited and doubly excited states shown in Tables I and II, respectively (see also Fig. 1). We emphasize that the energies in these tables are the field-free energies of these singly and doubly excited states; in the presence of the driving laser field, these energies may be shifted. Owing to its distance from the threshold, any shift of the ground-state energy by the laser field is expected to be small; however, the energy shifts of Rydberg states may be significant. Moreover, the driving laser pulse has a finite duration, which gives the three resonant frequencies a small bandwidth. None of these various considerations affect the results of our calculations of HHG for He, which are obtained by solving the full-dimensional, two-electron TDSE. However, these considerations will prove useful for understanding the results we obtain.

Table II shows that the He $2s2p(^1P)$ doubly excited state at around 59.9056 eV is not only relatively isolated from other doubly excited states but also has a relatively narrow width compared to some others. Specifically, its width is only $\Gamma = 0.03717$ eV [31], which corresponds to a relatively long lifetime of $\tau = 17.71$ fs. Note that this width, narrow as it is, is nevertheless more than 4 times larger than those of the group of doubly excited states below 65 eV, whose effect on the HHG spectrum of He was observed by Guan *et al.* [33]. The calculations of Ref. [33] employed a time-dependent generalized pseudospectral approach in hyperspherical coordinates, a KrF laser wavelength of 248.6 nm, a moderate laser intensity of $I = 10^{14}$ W/cm^2, and a relatively long driving laser pulse of

TABLE I. Energies of singly excited states of He.

	Absolute Energy (a.u.)			
	This work	Ref. [33]	Ref. [79]	E_{sg} (eV)[a]
	Ground-State Energy E_g			
$1s^2(^1S)$	$-2.895\,172$	$-2.903\,723$	$-2.903\,724$	0.000
	Singly excited state energy E_s			
$1s2s(^1S)$	$-2.145\,200$	$-2.145\,969$	$-2.145\,974$	20.41
$1s2p(^1P)$	$-2.123\,747$	$-2.123\,824$	$-2.123\,843$	21.00
$1s3s(^1S)$	$-2.060\,998$	$-2.061\,261$	$-2.061\,271$	22.70
$1s3p(^1P)$	$-2.055\,022$	$-2.055\,127$	$-2.055\,146$	22.86
$1s3d(^1D)$	$-2.055\,591$	$-2.055\,600$	$-2.055\,620$	22.85
$1s4s(^1S)$	$-2.028\,786$			23.58
$1s4p(^1P)$	$-2.025\,548$			23.66
$1s4d(^1D)$	$-2.028\,015$			23.60
$1s4f(^1F)$	$-2.030\,026$			23.54
$1s5g(^1G)$	$-2.013\,891$			23.98

[a] $E_{sg} \equiv E_s - E_g$ is the excitation energy (eV).

TABLE II. He $(n_1,n_2)\,^1L$ doubly excited state energies.

	Absolute energy E_d (a.u.)				
(n_1,n_2)	This work	Ref. [33]	Ref. [79]	E_{dg} (eV)[a]	Γ (eV)[b]
$(2,2)^1S$	−0.777 51	−0.777 81	−0.777 87	57.62	0.123 81
$(2,2)^1S$	−0.621 76	−0.621 95	−0.621 81	61.86	0.005 87
$(2,3)^1S$	−0.547 76	−0.548 05	−0.548 07	63.87	0.001 85
$(2,2)^1P$	−0.693 68	−0.693 21	−0.693 07	59.91	0.037 17
$(2,3)^1P$	−0.597 07	−0.597 04	−0.597 07	62.53	0.000 11
$(2,3)^1P$	−0.564 02	−0.564 04	−0.564 07	63.43	0.007 97
$(2,3)^1P$	−0.546 84	−0.547 07	−0.547 09	63.90	
	Absolute energy E_d (a.u.)				
(n_1,n_2)	This work	Ref. [31]	Ref. [80]	E_{dg} (eV)[a]	Γ (eV)[b]
$(3,3)^1P$	−0.338 286	−0.335 611	−0.335 627	69.58	0.188 30
$(3,3)^1P$	−0.285 865	−0.286 2	−0.285 951	71.00	0.008 27
$(3,3)^1P$	−0.282 920	−0.282 855	−0.282 829	71.08	0.044 35
	Absolute energy E_d (a.u.)				
(n_1,n_2)	This work	Ref. [31]	Ref. [81]	E_{dg} (eV)[a]	Γ (eV)[b]
$(2,3)^1F$	−0.558 222	−0.558 283	−0.558 828	63.59	0.000 35
$(2,3)^1F$	−0.530 311	−0.532 294		64.35	0.000 95
$(3,3)^1F$	−0.304 084	−0.304 247	−0.304 24	70.51	0.088 16
$(3,3)^1F$	−0.277 816	−0.278 003		71.22	0.002 61

[a] $E_{dg} \equiv E_d - E_g$ is the excitation energy (eV).
[b] The width Γ of the state E_d is taken from Ref. [31].

30 optical cycles (corresponding to a duration of 24.87 fs and a bandwidth of 0.0265 eV). In order to test the convergence of our approach in terms of the number of pairs of angular momenta employed as well as the number of total angular momenta, we have considered similar parameters to those used in the calculations of Guan *et al.* [33]. In Fig. 2 we show our results for the dipole velocity amplitude $d_V(t)$ [cf. Eqs. (16) and (17)] and the harmonic power $\mathcal{P}(\omega_L;\omega)$ [cf. Eq. (18)]. The latter is shown in Fig. 2(b) in the vicinity of the 11th, 13th, and 15th harmonics as a function of the number of angular momentum pairs. It is shown in Fig. 2(c) over the entire HHG spectrum as a function of the number of total angular momenta. These results show that for either the time-dependent dipole velocity amplitude or the harmonic power spectrum, good convergence has been achieved and the shape of the 13th harmonic, which is on resonance with the group of autoionizing states below 65 eV, agrees qualitatively with that obtained in Ref. [33].

Finally, Table III shows that for driving laser frequencies such that the 9th, 11th, or 13th harmonics are in resonance with the He $2s2p(^1P)$ autoionizing state, there exist lower-order harmonics that are close to resonance with singly excited states as well as higher-order harmonics (in the case of the 11th harmonic) in resonance with higher-energy doubly excited states. For a driving laser pulse with carrier frequency ω_L and bandwidth Δ there can be an overlap between $N(\omega_L \pm \Delta)$ and $E_{2s2p(^1P)} \pm \Gamma$ when the frequency is scanned. Of course, when the laser pulse is on, the energies of the excited resonance states may shift. Having such an overlap between the pulse bandwidth and the resonance position and width may increase the possibility for resonance effects on the HHG power spectrum to occur. We expect that when a resonance occurs for a lower-order harmonic (e.g., with a singly excited Rydberg level), all higher harmonics will experience an increase in the HHG power. This occurs in our results for the 9th and 13th harmonics. When higher harmonics are in resonance with higher-energy doubly excited states (as in our results for the 11th harmonic), we find the harmonics in resonance with the two doubly excited states compete for intensity.

C. Evidence of the He $2s2p(^1P)$ autoionizing state on resonant harmonics

In terms of the field-free He energy levels, the driving laser frequencies at which the 9th, 11th, and 13th harmonics

TABLE III. Driving laser frequencies $\omega_L^{\rm res}(N)$ in N-photon resonance with the He $2s2p(^1P)$ autoionizing resonance $\omega_L^{\rm res}(N) = E_{2s2p(^1P)}/N$ and their harmonics $n\omega_L^{\rm res}(N)$ for $N = 9$, 11, and 13.

	Harmonic energy (eV)[a]		
Harmonic n	$n\omega_L^{\rm res}(9)$	$n\omega_L^{\rm res}(11)$	$n\omega_L^{\rm res}(13)$
1	6.65618	5.44596	4.60812
3	**19.9685**	16.3379	13.8244
5	33.2809	27.2298	**23.0406**
7	46.5932	38.1217	32.2569
9	**59.9056**	49.0137	41.4731
11	73.2180	**59.9056**	50.6894
13	86.5303	**70.7975**	**59.9056**
15	99.8427	81.6895	69.1218
17	113.1550	92.5814	78.3381

[a] Harmonic energies in bold are close to singly or doubly excited state excitation energies (cf. Tables I and II).

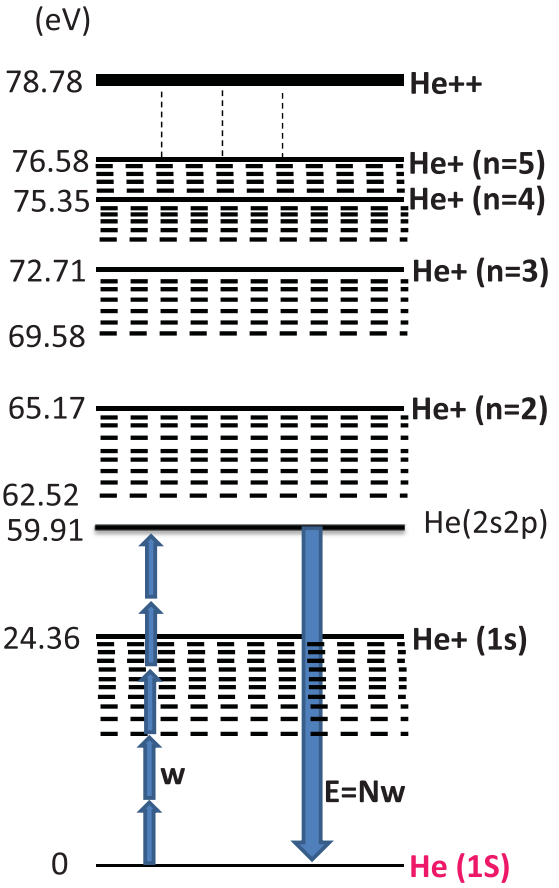

FIG. 1. (Color online) Energy level diagram showing the field-free singly and doubly excited states of He, with excitation energies (in eV) above the (approximate) ground-state energy of −2.895 172 a.u. Note that the He $(2s2p)^1P$ autoionizing state has an excitation energy of 59.9056 eV. The blue arrows indicate a multiphoton transition to the He $(2s2p)^1P$ autoionizing state followed by harmonic emission back to the ground state.

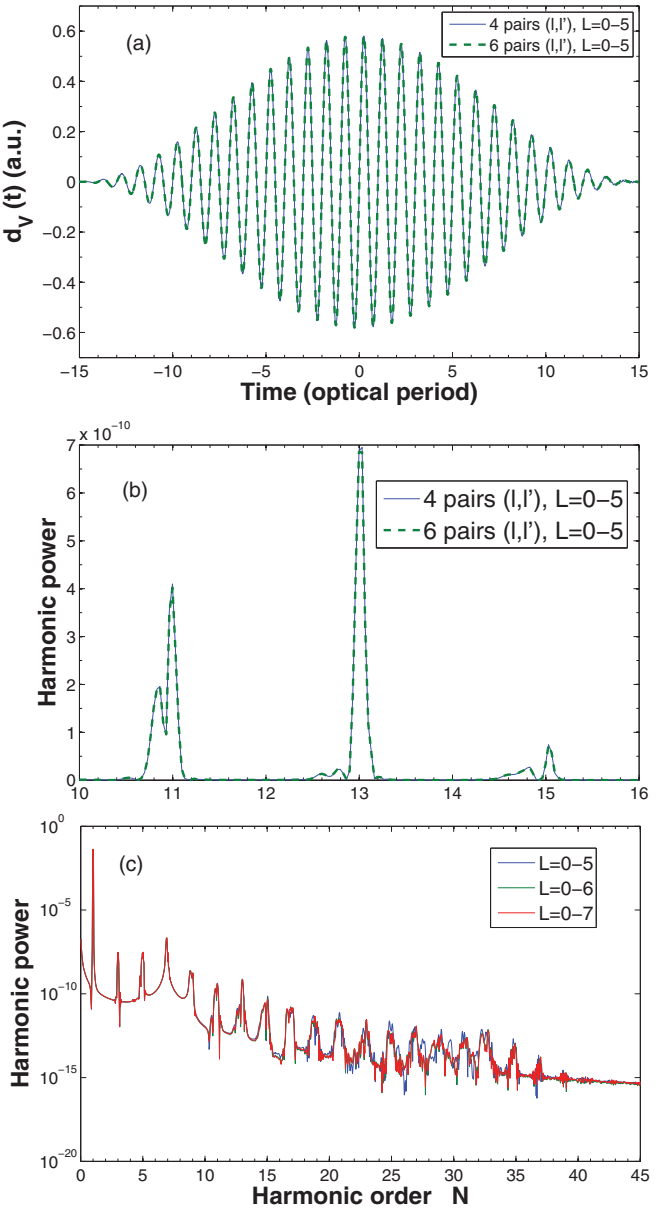

FIG. 2. (Color online) Convergence tests of our results. (a) Time-dependent dipole velocity amplitude $d_V(t)$ (a.u.) [cf. Eqs. (16) and (17)] for a cosine squared driving laser pulse vs number of orbital angular momentum pairs. (b) Harmonic power $\mathcal{P}(\omega_L;\omega)$ (a.u.) [cf. Eq. (18)] around the 13th harmonic (which is in resonance with the group of autoionizing states below 65 eV) vs number of orbital angular momentum pairs for a driving laser frequency $\omega_L = 5$ eV, a laser peak intensity of $I = 10^{14}$ W/cm^2, and 30 optical cycles. (c) Harmonic power $\mathcal{P}(\omega_L;\omega)$ (a.u.) spectrum vs number of total angular momenta L for the same laser parameters as in (b).

are in resonance with the He $2s2p(^1P)$ autoionizing state are $\omega_L^{\rm res}(9) = 6.656\,18$ eV, $\omega_L^{\rm res}(13) = 5.44596$ eV, and $\omega_L^{\rm res}(13) = 4.6081$ eV. Figures 3, 4, and 5 present (on a linear scale) the harmonic power in the neighborhood of the 9th, 11th, and 13th harmonics, respectively, for a range of driving laser frequencies ω_L below, equal to, and above the corresponding resonant frequency $\omega_L^{\rm res}(N)$.

For the laser intensity $I = 10^{14}$ W/cm^2 used in our calculations and for the driving laser frequencies $\omega_L^{\rm res}(N)$ for which the $N = 9$, 11, and 13 harmonics are in resonance with the He $2s2p(^1P)$ autoionizing state, the Keldysh parameter γ takes the values 6.16, 5.04, and 4.26, respectively. Hence, our calculations are for the multiphoton regime, and we expect that the intensities of successive harmonics will decrease with harmonic order. In Figs. 3(a), 4(a), and 5(a), one sees that for driving laser frequencies below resonance this is, in fact, the case. For the 9th and 13th harmonics, Figs. 3(d) and 5(d) show that this is also the case for driving laser frequencies above resonance. However, for the 9th and 13th harmonics, when the driving laser frequency is close to and on resonance, the harmonic intensity becomes much greater than that of its nearest neighbors [cf. Figs. 3(b), 3(c), 5(b), and 5(c)]. Moreover, the intensity profiles of the harmonics near and on resonance are asymmetric, as are, in general, the profiles of autoionizing states [82], although the connection between the two is at this point merely suggestive. The maximum peak heights of the 9th and 13th harmonics occur just below the resonance frequency, as will be discussed later.

Surprisingly, the resonance effect in the case of the 11th harmonic, shown in Figs. 4(b) and 4(c), is less apparent than for the 9th and 13th harmonics. Moreover, above the

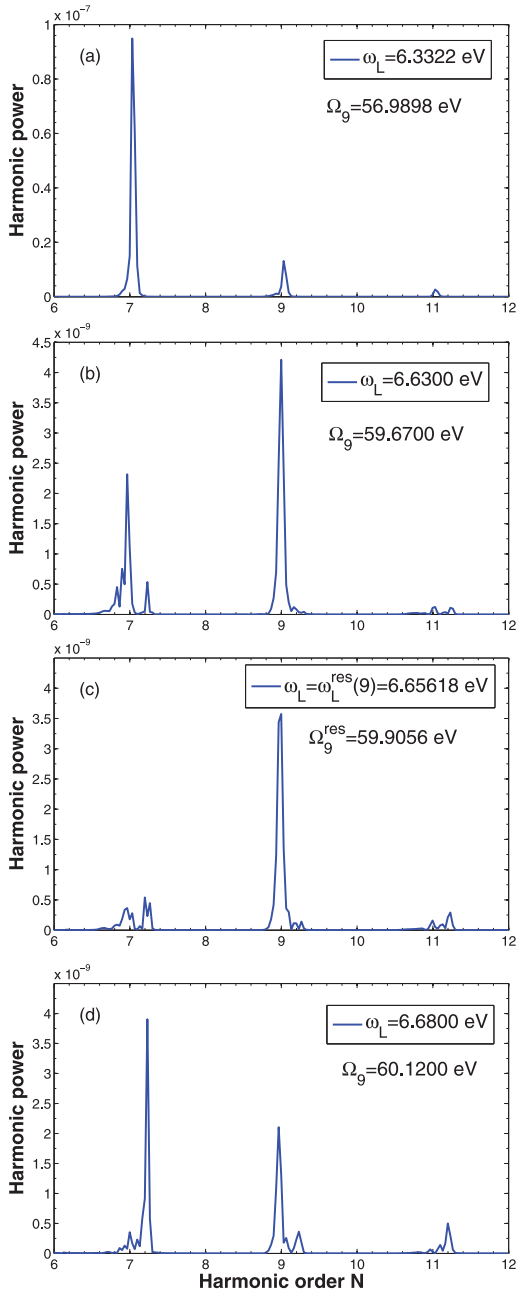

FIG. 3. (Color online) Harmonic power $\mathcal{P}(\omega_L;\omega)$ (a.u.) [cf. Eq. (18)] for the 9th harmonic (and its two nearest neighbors) for four driving laser frequencies ω_L that put the 9th harmonic frequency $\Omega_9 \equiv 9\omega_L$ below, above, and in resonance with the He $2s2p(^1P)$ autoionizing state. The harmonic order $N \equiv \omega/\omega_L$. The laser pulse peak intensity is $I = 10^{14}$ W/cm^2, and the shape is trapezoidal.

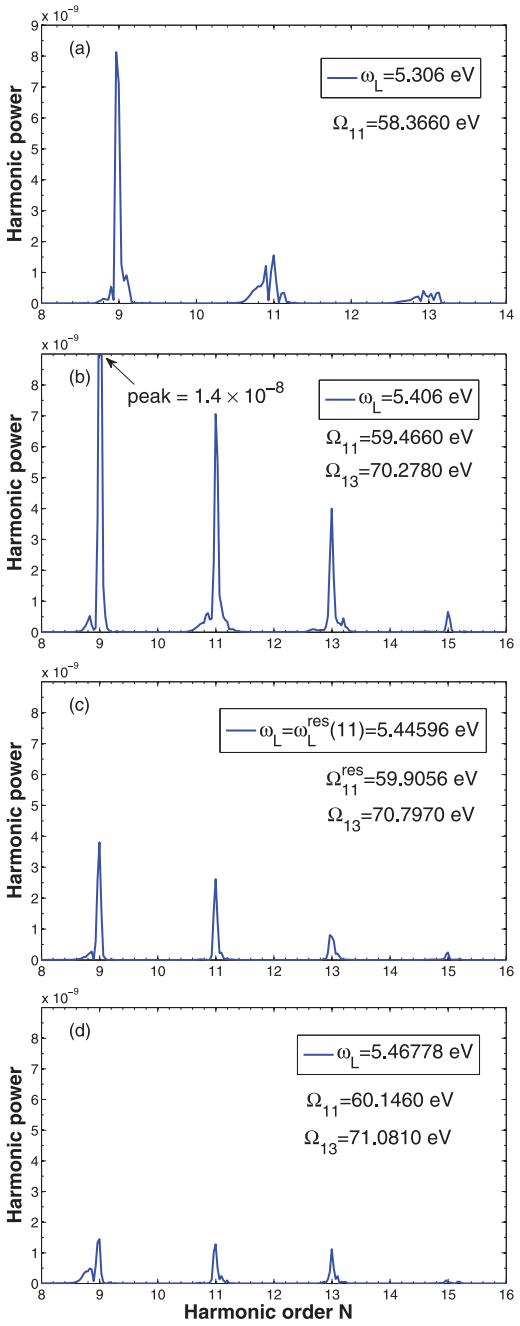

FIG. 4. (Color online) Harmonic power $\mathcal{P}(\omega_L;\omega)$ (a.u.) [cf. Eq. (18)] for the 11th harmonic (and its two nearest neighbors) for four driving laser frequencies ω_L that put the 11th harmonic frequency $\Omega_{11} \equiv 11\omega_L$ below, above, and in resonance with the He $2s2p(^1P)$ autoionizing state. The harmonic order $N \equiv \omega/\omega_L$. The laser pulse peak intensity is $I = 10^{14}$ W/cm^2, and the shape is trapezoidal.

resonance frequency for the 11th harmonic [cf. Fig. 4(d)], the 9th, 11th, and 13th harmonics all have comparable intensities. A clue to this anomalous behavior is that the frequency Ω_{13} of the 13th harmonic in Figs. 4(b), 4(c), and 4(d) lies in the vicinity of the doubly excited ^1P and ^1F states below the $He^+(n = 3)$ threshold (cf. Tables II and III and Fig. 1), so that the intensity of the 13th harmonic may be expected to increase owing to this resonance. With only a two-photon transition coupling the doubly excited states to which the 11th and 13th harmonics are resonant, one might expect part of the intensity of the resonant 11th harmonic (with the He $2s2p(^1P)$ autoionizing state) would be transferred to the resonant 13th harmonic (with the autoionizing states below the $He^+(n = 3)$ threshold). Such laser coupling between autoionizing states has been discussed theoretically in Ref. [61]. Such coupling has also been observed experimentally recently in Ar [71]. Although neither reference deals with harmonic generation, both show that the strong interaction between resonantly coupled autoionizing states can influence atomic processes.

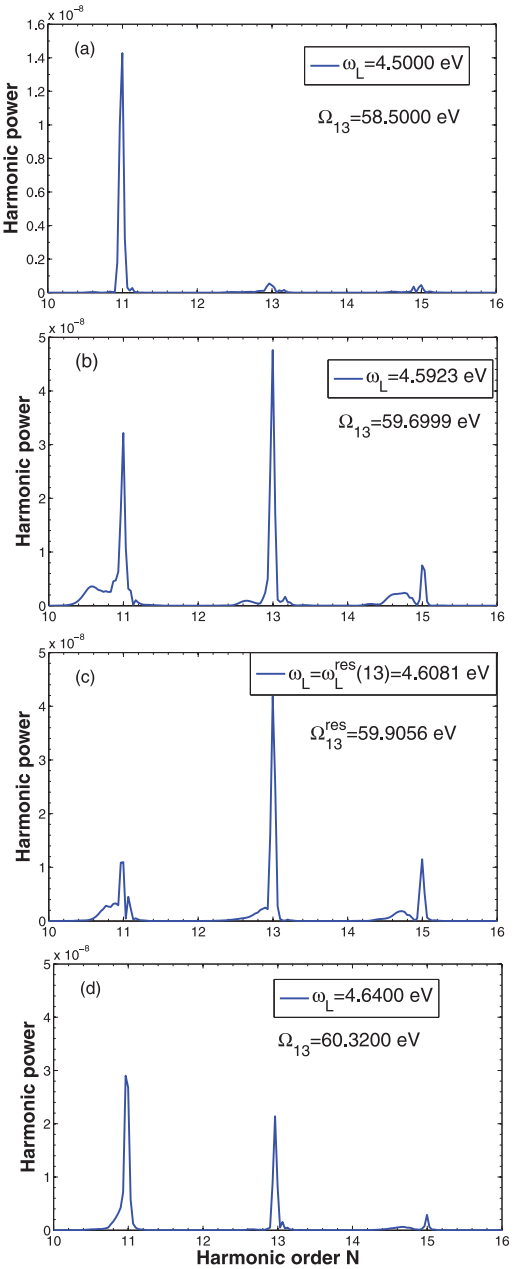

FIG. 5. (Color online) Harmonic power $\mathcal{P}(\omega_L;\omega)$ (a.u.) [cf. Eq. (18)] for the 13th harmonic (and its two nearest neighbors) for four driving laser frequencies ω_L that put the 13th harmonic frequency $\Omega_{13} \equiv 13\omega_L$ below, above, and in resonance with the He $2s2p(^1P)$ autoionizing state. The harmonic order $N \equiv \omega/\omega_L$. The laser pulse peak intensity is $I = 10^{14}$ W/cm^2, and the shape is trapezoidal.

Thus, in our case, the resonant 11th harmonic may be considered as an intermediate (resonant) step for the resonant 13th harmonic, coupling different autoionizing resonances.

For the two harmonics in which resonance with the He $2s2p(^1P)$ autoionizing state is clearly observed (i.e., $N = 9$, 13), it is useful to calculate the integrated harmonic power A_N of the Nth harmonic, which is given by

$$A_N(\omega_L) = \int_{(N-1)\omega_L}^{(N+1)\omega_L} \mathcal{P}(\omega_L;\omega)\, d\omega. \tag{19}$$

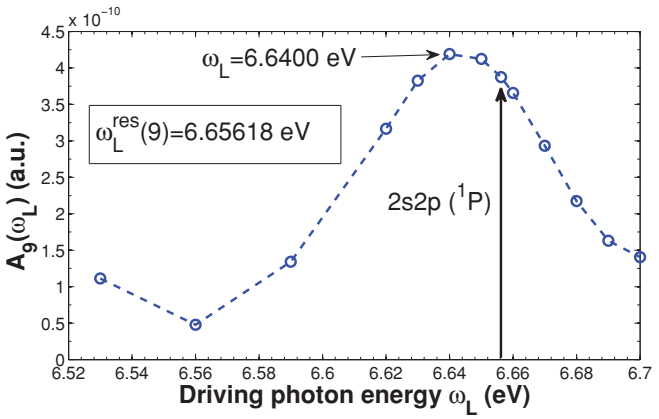

FIG. 6. (Color online) Variation of the integrated harmonic power $A_9(\omega_L)$ [cf. Eq. (19)] of the 9th harmonic with driving laser frequency ω_L. The vertical arrow marks $\omega_L = \omega_L^{\rm res}(9)$, at which the 9th harmonic is resonant with the He $2s2p(^1P)$ state.

Figure 6 shows the variation of $A_9(\omega_L)$ as a function of the driving laser frequency ω_L. The maximum in Fig. 6 is very broad and is located at $\omega_L = 6.64$ eV, which is close to, but not exactly at, the resonant frequency $\omega_L^{\rm res}(9) = 6.656\,18$ eV. The 9th harmonic for the peak frequency is thus $\approx$0.15 eV below that of $\Omega_9^{\rm res}$. Moreover, the width of the peak is much broader than that of the He $2s2p(^1P)$ state (cf. Table II), thus indicating the involvement of additional resonant transitions. Tables I and III and Fig. 1 in fact show that for such frequencies ω_L the three-photon transition from the He ground state lies about 1 eV below the $1s2p(^1P)$ excited state (located at 21 eV).

In the case of $A_{13}(\omega_L)$, shown in Fig. 7, there exist two local maxima. The highest one is at $\omega_L = 4.6175$ eV, which corresponds to a 13th harmonic frequency Ω_{13} that is $\approx$0.12 eV above the energy of the He $2s2p(^1P)$ state. The lower maximum is at $\omega_L = 4.59$ eV, which corresponds to a 5th harmonic that is only 0.09 eV above the He $1s3p(^1P)$ state (cf. Table I). Similar to the results in Fig. 6 for $A_9(\omega_L)$, the width of the entire structure in Fig. 7 is about twice the width of the He $2s2p(^1P)$ state; however, the width of only the higher-energy peak structure is comparable. Thus in this case as well, the involvement of additional resonance transitions complicates the analysis.

In order to isolate the effect of the He $2s2p(^1P)$ state on the above two resonant harmonics, we show in Figs. 8 and 9 the integrated harmonic power ratios $A_N(\omega_L)/A_{N-2}(\omega_L)$ for $N = 9,13$. In these ratios, the He $2s2p(^1P)$ state should not affect significantly the denominators since it is the Nth harmonic that is in resonance and not the $(N-2)$ harmonic. On the other hand, low-order multiphoton resonances with singly excited states of He will affect both the numerator and denominator. Hence, taking the ratio essentially removes the influence of the singly excited state resonances so that the structure in the ratio originates essentially entirely from the autoionizing state.

The results in Figs. 8 and 9 clearly show that these expectations are realized. In each case the ratio exhibits a single asymmetric peak with a narrow energy width. For the ratio $A_9(\omega_L)/A_7(\omega_L)$, shown in Fig. 8, we present results for two different 30-cycle laser pulse shapes, trapezoidal and Gaussian. As expected the greater monochromaticity of the

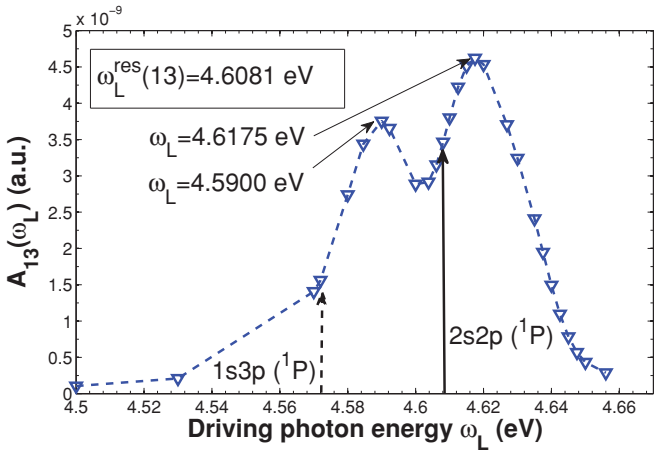

FIG. 7. (Color online) Variation of the integrated harmonic power $A_{13}(\omega_L)$ [cf. Eq. (19)] of the 13th harmonic with driving laser frequency ω_L. The solid vertical arrow marks $\omega_L = \omega_L^{\rm res}(13)$, at which the 13th harmonic is resonant with the He $2s2p(^1P)$ state. The dashed vertical arrow marks the frequency $\omega_L = 4.572$ eV at which the 5th harmonic Ω_5 is resonant with the field-free energy of the He $1s3p(^1P)$ singly excited state.

trapezoidal pulse reveals the resonance much more clearly than the higher-bandwidth Gaussian pulse. For the trapezoidal pulse, the ratio has a peak height of 3.8, whereas the Gaussian pulse peak height is only 1.6. Moreover, the peak of the trapezoidal result is exactly on resonance with the autoionizing state, whereas that of the Gaussian pulse is shifted ≈0.16 eV higher. Each has a width Γ_9 (shown in Fig. 8) that is comparable to that of the autoionizing state, which is 0.037 eV. For the ratio $A_{13}(\omega_L)/A_{11}(\omega_L)$, shown in Fig. 9, the peak maximum of 3.0 is located ≈0.09 eV higher than that of the field-free autoionizing resonance, and the width is a bit smaller, but of the same magnitude. We observe also that in both Figs. 8 and 9 the asymmetries are similar to those observed in the energy-loss measurements of Silverman and Lassettre (cf. Figs. 2 and 3 of Ref. [82]).

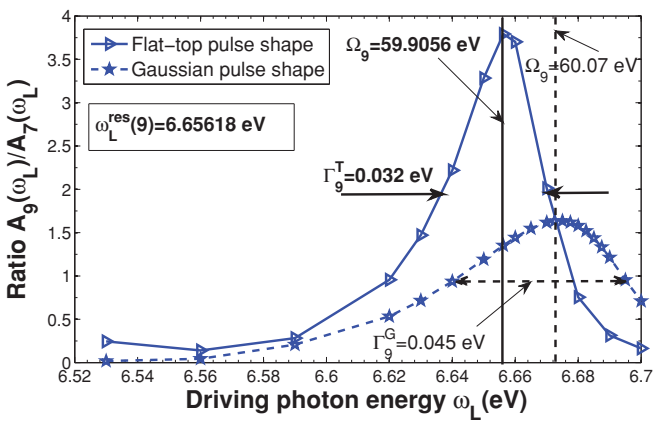

FIG. 8. (Color online) Integrated harmonic power ratio $A_9(\omega_L)/A_7(\omega_L)$ for two different 30-cycle laser pulse shapes, trapezoidal (solid curve) and Gaussian (dashed curve). See text for details.

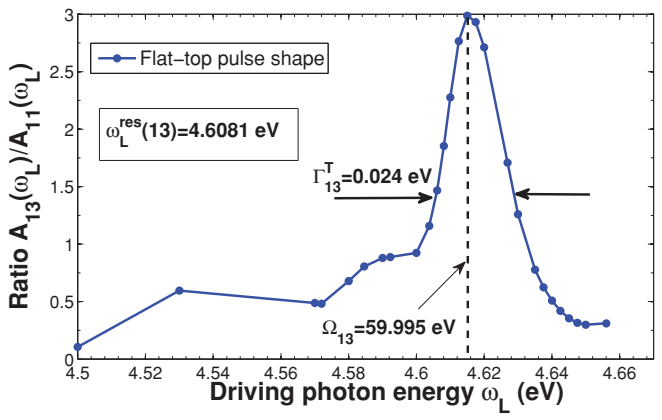

FIG. 9. (Color online) Integrated harmonic power ratio $A_{13}(\omega_L)/A_{11}(\omega_L)$ for a 30-cycle, trapezoidal-shaped laser pulse.

The case of the 11th harmonic in the vicinity of its resonance with the He $2s2p(^1P)$ state is complicated by the fact that in the vicinity of $\omega_L^{\rm res}(11)$ the 13th harmonic is in resonance with odd-parity doubly excited states below the $He^+(n = 3)$ threshold (cf. Tables II and III and Fig. 1). Hence, the He $2s2p(^1P)$ autoionizing state and those below the $He^+(n = 3)$ threshold are coupled by a two-photon transition, consequently diminishing the intensity of the 11th harmonic by "feeding" the intensity of the 13th harmonic. Recall that unlike the 9th and 13th harmonics, whose harmonic powers become much larger than those of their neighboring harmonics in the vicinity of their resonance frequencies, the 11th harmonic's power does not (cf. Figs. 3, 4, and 5). Competition between the 11th and the 13th harmonics for intensity may thus be present.

In Fig. 10 we compare the two ratios $A_{11}(\omega_L)/A_9(\omega_L)$ and $A_{13}(\omega_L)/A_9(\omega_L)$ for driving laser frequencies in the vicinity of $\omega_L^{\rm res}(11)$. We take the integrated harmonic power ratios of A_{11} and A_{13} with A_9 since the 9th harmonic is not in resonance with any doubly excited states (and also to remove effects of any low-order multiphoton resonance with singly excited states that may be present). One sees that the 11th harmonic

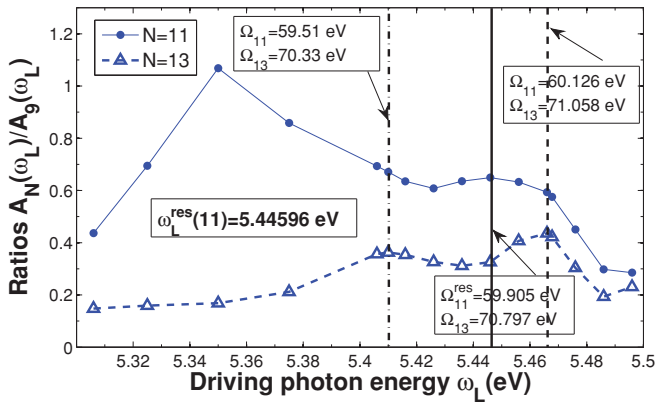

FIG. 10. (Color online) Integrated harmonic power ratios $A_N(\omega_L)/A_9(\omega_L)$ for $N = 11$ (solid curve) and $N = 13$ (dashed curve) for a 30-cycle, trapezoidal-shaped laser pulse. The solid vertical line shows $\omega_L^{\rm res}(11)$, at which the 11th harmonic is resonant with the He $2s2p(^1P)$ state. The dash-dotted and dashed vertical lines indicate the frequencies of the two maxima of the $N = 13$ ratio.

does indeed have a local maximum at its resonance frequency. However, as the frequency increases, the magnitude of the 11th harmonic ratio drops while that of the 13th harmonic ratio increases and soon reaches a local maximum. At this maximum, $\Omega_{13} = 71.058$ eV lies between two ^1P doubly excited states below the $He^+(n = 3)$ threshold. For $\omega_L = 5.41$ eV, the curve for $N = 13$ has a local maximum corresponding to $\Omega_{13} = 70.33$ eV, which lies just 0.18 eV below a ^1F doubly excited state associated with the He^+ $(n = 3)$ threshold. (We are not able to explain the maximum in the $N = 11$ curve at $\omega_L = 5.35$ eV; we note simply that for this frequency there is a 12-photon resonance with even-parity doubly excited states below the $He^+(n = 2)$ threshold and also that this clearly does not involve the He $2s2p(^1P)$ state that is the focus of this paper.)

In Fig. 11 we show how the results for the integrated harmonic power of the ninth harmonic $A_9(\omega_L)$ and of the integrated harmonic power ratio $A_9(\omega_L)/A_7(\omega_L)$ vary with the intensity of the driving laser field. The solid curves are the results for a laser pulse peak intensity of $I = 10^{14}$ W/cm^2 that were shown previously in Figs. 6 and 8, respectively. The other curves give results for three lower and two higher intensities. In all cases, the pulse shape is trapezoidal. One sees clearly that resonance is predicted for each of the six intensities shown [even for the lowest intensity, which is difficult to see in Fig. 11(a) on the scale shown but is seen in Fig. 11(b)].

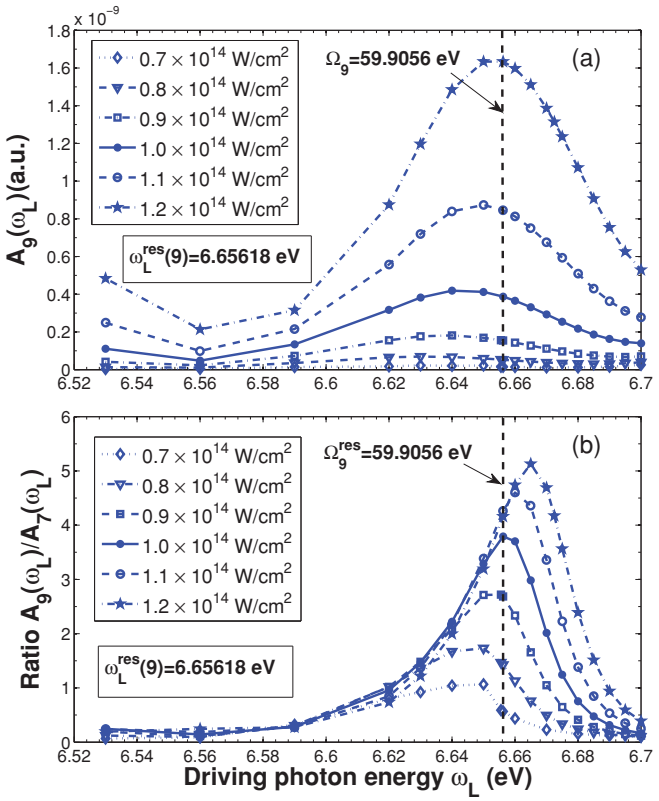

FIG. 11. (Color online) Intensity dependence of (a) the integrated harmonic power $A_9(\omega_L)$ [cf. Eq. (19)] of the 9th harmonic and of (b) the integrated harmonic power ratio $A_9(\omega_L)/A_7(\omega_L)$. For each of the six intensities shown, the results are plotted as a function of the driving laser frequency ω_L. The vertical dashed line marks $\omega_L = \omega_L^{res}(9)$, at which the 9th harmonic is resonant with the He $2s2p(^1P)$ state.

Most striking is that the energy position of the resonance is only weakly dependent on the peak laser intensity, varying with intensity over an energy range that is considerably smaller than the energy widths of the integrated harmonic power profiles.

IV. SUMMARY AND CONCLUSIONS

In summary, we have solved the fully dimensional time-dependent Schrödinger equation for a two-active-electron system (helium) in an intense and ultrashort laser field in order to study the role of electron correlation in the resonant enhancement of some harmonics in the HHG spectrum. Whereas in the tunneling regime the HHG rate has been shown to be proportional to the field-free photorecombination cross section (and hence to exhibit any correlation features in that cross section), the parameters of our present calculation are in the multiphoton regime, for which such a proportionality has not been predicted. However, based on perturbation theory arguments, electron correlations should be expected to play a role.

Our nonperturbative numerical calculations have focused on identifying signatures of the well-isolated He $2s2p(^1P)$ autoionizing state on the 9th, 11th, and 13th harmonics for a range of driving laser frequencies ω_L that put these harmonics in resonance with that state (from the ground state). Despite the fact that He is the simplest and most fundamental multielectron system, our results show that isolating the resonant enhancement of the particular harmonics we investigated is complicated by both low-order multiphoton resonances with singly excited states and also by resonant coupling between different autoionizing states. Nevertheless, our results show that when resonant coupling between doubly excited states is absent, the resonant enhancement of the He $2s2p(^1P)$ autoionizing state on the 9th and 13th harmonics is clearly observable when one examines the ratio of the harmonic powers of these two harmonics with those of their lower-order neighboring harmonics. These ratios serve to remove the effect of low-order multiphoton resonances with singly excited states and thus isolate the effect of the resonance with the autoionizing state.

For the case of a 30-cycle trapezoidal laser pulse [with 8-cycle ramps (up and down) and a 14-cycle flat top], our results show that whereas below and above resonance with the He $2s2p(^1P)$ autoionizing state the ratios of the 9th harmonic to the 7th harmonic and of the 13th harmonic to the 11th harmonic are much less than unity, on resonance these ratios increase to a range of 3–4 for a laser intensity of 10^{14} W/cm^2. For a range of intensities about this latter value, the ratio of the 9th to the 7th harmonic on resonance ranges from 1 to 5 (cf. Fig. 11). Moreover, the width of the maximum is comparable to that of the He $2s2p(^1P)$ autoionizing state. For a 30-cycle Gaussian pulse, an increase in these ratios is also found, but it is spread over a wider range of frequencies and reaches a maximum of less than 2 for a laser intensity of 10^{14} W/cm^2. These results indicate the necessity of having as close to a monochromatic driving laser pulse as possible in order to probe narrow correlation features in HHG spectra. When this is the case, our results demonstrate that electron correlations occurring over a narrow energy interval can indeed have a

significant effect on strong-field processes such as harmonic generation.

Experimental observation of the results presented here seems feasible for experiments employing a spatially shaped (flat-top) focus, as in the experiment of Toma *et al.* [77]. However, even for a Gaussian-shaped driving laser pulse, our results in Fig. 8 show that resonance behavior as a function of driving laser frequency may be observable. We have shown results as a function of driving laser frequency in the narrow frequency range 4.6 eV $\leqslant \hbar\omega_L \leqslant$ 6.6 eV, within which lie the fundamental frequency of the KrF laser and the 3rd, 4th, and 5th harmonics of the tunable Ti:sapphire laser. Only a small variation of the driving laser frequency is sufficient to scan the peak of the predicted resonances. Moreover, as shown in Fig. 11, the results appear to be reasonably insensitive to variations of intensity. In particular, the energy shift of the resonance maxima with driving laser intensity appears to be smaller in magnitude than the width of the resonance profile.

In principle, the influence of autoionizing states on HHG spectra should be observable also in the tunneling regime for a monochromatic driving laser field. Indeed, as noted already, an experiment using a double-optical-gating technique and laser peak intensities in the tunneling regime (i.e., 0.9–1.7 $\times 10^{15}$ W/cm^2) observed a "prominent peak" in the He harmonic supercontinuum spectrum at a photon energy of $\approx$60 eV, which the authors attributed to the He $2s2p(^1P)$ autoionization state [73]. Unfortunately, *ab initio* calculation of such two-electron effects in the tunneling regime is difficult for He owing both to the large number of photons needed in this regime to reach doubly excited states and to the large values of driving laser intensity necessary to produce a harmonic plateau. Other effective "two-electron" systems (e.g., Be or Mg) may prove to be numerically feasible, as their doubly excited states lie much lower in energy above their ground states. Finally, although the connection between the HHG spectrum and the field-free photorecombination cross section (as well as the proportionally related field-free photoionization cross section) has been proved analytically for a model system [12] and shown to be applicable also for real systems (see Refs. [7–11,13–16,20]), no such analysis has been done for the multiphoton regime. Thus, the fact that the resonance profiles we have predicted here have asymmetric shapes, just as in field-free atomic cross section data for reactions in the vicinity of an autoionizing resonance, suggests that such a connection may exist also in the multiphoton regime. Of course, our results certainly do not prove this connection, but instead provide an incentive for further analysis to show whether or not such a connection exists.

ACKNOWLEDGMENTS

Useful discussions with M. V. Frolov and N. L. Manakov are gratefully acknowledged. This work is supported in part by the US Department of Energy, Office of Science, Division of Chemical Sciences, Geosciences, and Biosciences, under Grant No. DE-FG03-96ER14646.

[1] P. B. Corkum and F. Krausz, Nat. Phys. **3**, 381 (2007).
[2] F. Krausz and M. Ivanov, Rev. Mod. Phys. **81**, 163 (2009).
[3] P. B. Corkum,Phys. Today **64** (3), 36 (2011).
[4] K. J. Schafer, B. Yang, L. F. DiMauro, and K. C. Kulander, Phys. Rev. Lett. **70**, 1599 (1993).
[5] P. B. Corkum, Phys. Rev. Lett. **71**, 1994 (1993).
[6] M. Lewenstein, Ph. Balcou, M. Yu. Ivanov, A. L'Huillier, and P. B. Corkum, Phys. Rev. A **49**, 2117 (1994).
[7] T. Morishita, A.-T. Le, Z. Chen, and C. D. Lin, Phys. Rev. Lett. **100**, 013903 (2008).
[8] A.-T. Le, T. Morishita, and C. D. Lin, Phys. Rev. A **78**, 023814 (2008).
[9] S. Minemoto, T. Umegaki, Y. Oguchi, T. Morishita, A.-T. Le, S. Watanabe, and H. Sakai, Phys. Rev. A **78**, 061402(R) (2008).
[10] H. J. Wörner, H. Niikura, J. B. Bertrand, P. B. Corkum, and D. M. Villeneuve, Phys. Rev. Lett. **102**, 103901 (2009).
[11] C. D. Lin, A.-T. Le, Z. Chen, T. Morishita, and R. Lucchese, J. Phys. B **43**, 122001 (2010).
[12] M. V. Frolov, N. L. Manakov, T. S. Sarantseva, and A. F. Starace, J. Phys. B **42**, 035601 (2009); Phys. Rev. A **83**, 043416 (2011).
[13] M. V. Frolov, N. L. Manakov, T. S. Sarantseva, M. Yu. Emelin, M. Yu. Ryabikin, and A. F. Starace, Phys. Rev. Lett. **102**, 243901 (2009).
[14] M. V. Frolov, N. L. Manakov, A. A. Silaev, and N. V. Vvedenskii, Phys. Rev. A **81**, 063407 (2010).
[15] M. V. Frolov, N. L. Manakov, A. A. Silaev, N. V. Vvedenskii, and A. F. Starace, Phys. Rev. A **83**, 021405(R) (2011).
[16] A. D. Shiner, B. E. Schmidt, C. Trallero-Herrero, H. J. Wörner, S. Patchkovskii, P. B. Corkum, J.-C. Kieffer, F. Légaré, and D. M. Villeneuve, Nat. Phys. **7**, 464 (2011).
[17] R. A. Ganeev, L. B. Elouga Bom, J.-C. Kieffer, and T. Ozaki, Phys. Rev. A **75**, 063806 (2007).
[18] R. A. Ganeev, M. Suzuki, M. Baba, and H. Kuroda, Phys. Rev. A **76**, 023805 (2007).
[19] R. A. Ganeev, J. Phys. B **40**, R213 (2007); Usp. Fiz. Nauk **179**, 65 (2009) [Phys. Usp. **52**, 55 (2009)].
[20] M. V. Frolov, N. L. Manakov, and A. F. Starace, Phys. Rev. A **82**, 023424 (2010).
[21] Z. Chang, A. Rundquist, H. Wang, M. M. Murnane, and H. C. Kapteyn, Phys. Rev. Lett. **79**, 2967 (1997).
[22] C. Spielmann, N. H. Burnett, S. Sartania, R. Koppitsch, M. Schnürer, C. Kan, M. Lenzner, P. Wobrauschek, and F. Krausz, Science **278**, 661 (1997).
[23] M.-C. Chen, P. Arpin, T. Popmintchev, M. Gerrity, B. Zhang, M. Seaberg, D. Popmintchev, M. M. Murnane, and H. C. Kapteyn, Phys. Rev. Lett. **105**, 173901 (2010).
[24] P. Lambropoulos, P. Maragakis, and J. Zhang, Phys. Rep. **305**, 203 (1998).
[25] J. Parker, K. T. Taylor, C. W. Clark, and S. Blodgett-Ford, J. Phys. B **29**, L33 (1996).
[26] D. G. Lappas, A. Sanpera, J. B. Watson, K. Burnett, P. L. Knight, R. Grobe, and J. H. Eberly, J. Phys. B **29**, L619 (1996).

[27] N. Moiseyev and F. Weinhold, Phys. Rev. Lett. **78**, 2100 (1997).
[28] A. Scrinzi and B. Piraux, Phys. Rev. A **56**, R13 (1997).
[29] X.-M. Tong and Shih I. Chu, Phys. Rev. A **57**, 452 (1998).
[30] C. A. Nicolaides, S. Dionissopoulou, and Th. Mercouris, J. Phys. B **31**, L1 (1998).
[31] A. Scrinzi and B. Piraux, Phys. Rev. A **58**, 1310 (1998).
[32] S. Dionissopoulou, Th. Mercouris, and C. A. Nicolaides, Phys. Rev. A **61**, 063402 (2000).
[33] X. Guan, X.-M. Tong, and Shih I. Chu, Phys. Rev. A **73**, 023403 (2006).
[34] A. Gordon, F. X. Kärtner, N. Rohringer, and R. Santra, Phys. Rev. Lett. **96**, 223902 (2006).
[35] A. Saenz and P. Lambropoulos, J. Phys. B **32**, 5629 (1999).
[36] D. H. Glass and P. G. Burke, J. Phys. B **33**, 407 (2000).
[37] J. S. Parker, L. R. Moore, E. S. Smyth, and K. T. Taylor, J. Phys. B **33**, 1057 (2000).
[38] J. S. Parker, D. H. Glass, L. R. Moore, E. S. Smyth, K. T. Taylor, and P. G. Burke, J. Phys. B **33**, L239 (2000).
[39] K. T. Taylor, J. S. Parker, D. Dundas, K. J. Meharg, L.-Y. Peng, B. J. S. Doherty, and J. F. McCann, Phys. Scr., T **110**, 154 (2004).
[40] H. W. van der Hart, B. J. S. Doherty, J. S. Parker, and K. T. Taylor, J. Phys. B **38**, L207 (2005).
[41] H. W. van der Hart, Phys. Rev. A **73**, 023417 (2006).
[42] M. Madine and H. W. van der Hart, J. Phys. B **39**, 4049 (2006).
[43] M. S. Pindzola and F. Robicheaux, J. Phys. B **31**, L823 (1998).
[44] L. A. A. Nikolopoulos and P. Lambropoulos, J. Phys. B **34**, 545 (2001); **40**, 1347 (2007).
[45] M. G. Makris, L. A. A. Nikolopoulos, and P. Lambropoulos, Europhys. Lett. **54**, 722 (2001).
[46] J. Colgan and M. S. Pindzola, Phys. Rev. Lett. **88**, 173002 (2002).
[47] L. Feng and H. W. van der Hart, J. Phys. B **36**, L1 (2003).
[48] B. Piraux, J. Bauer, S. Laulan, and H. Bachau, Eur. Phys. J. D **26**, 7 (2003).
[49] S. X. Hu, J. Colgan, and L. A. Collins, J. Phys. B **38**, L35 (2005).
[50] S. X. Hu and L. A. Collins, Phys. Rev. Lett. **96**, 073004 (2006).
[51] A. Y. Istomin, E. A. Pronin, N. L. Manakov, S. I. Marmo, and A. F. Starace, Phys. Rev. Lett. **97**, 123002 (2006).
[52] E. Foumouo, G. L. Kamta, G. Edah, and B. Piraux, Phys. Rev. A **74**, 063409 (2006).
[53] I. A. Ivanov and A. S. Kheifets, Phys. Rev. A **75**, 033411 (2007).
[54] E. A. Pronin, N. L. Manakov, S. I. Marmo, and A. F. Starace, J. Phys. B **40**, 3115 (2007).
[55] E. Foumouo, Ph. Antoine, B. Piraux, L. Malegat, H. Bachau, and R. Shakeshaft, J. Phys. B **41**, 051001 (2008).
[56] A. Palacios, T. N. Rescigno, and C. W. McCurdy, Phys. Rev. A **77**, 032716 (2008); **79**, 033402 (2009); Phys. Rev. Lett. **103**, 253001 (2009).
[57] J. Feist, S. Nagele, R. Pazourek, E. Persson, B. I. Schneider, L. A. Collins, and J. Burgdörfer, Phys. Rev. A **77**, 043420 (2008).
[58] D. A. Horner, C. W. McCurdy, and T. N. Rescigno, Phys. Rev. A **78**, 043416 (2008).
[59] J. Feist, R. Pazourek, S. Nagele, E. Persson, B. I. Schneider, L. A. Collins, and J. Burgdörfer, J. Phys. B **42**, 134014 (2009).
[60] D. A. Horner, T. N. Rescigno, and C. W. McCurdy, Phys. Rev. A **81**, 023410 (2010).
[61] P. Lambropoulos and P. Zoller, Phys. Rev. A **24**, 379 (1981).
[62] S. Cavalieri and R. Eramo, Phys. Rev. A **58**, R4263 (1998).
[63] L. A. A. Nikolopoulos, T. Nakajima, and P. Lambropoulos, Eur. Phys. J. D **20**, 297 (2002).
[64] M. Wickenhauser, J. Burgdörfer, F. Krausz, and M. Drescher, Phys. Rev. Lett. **94**, 023002 (2005).
[65] Z. X. Zhao and C. D. Lin, Phys. Rev. A **71**, 060702(R) (2005).
[66] S. X. Hu and L. A. Collins, Phys. Rev. A **71**, 062707 (2005).
[67] Th. Mercouris, Y. Komninos, and C. A. Nicolaides, Phys. Rev. A **75**, 013407 (2007).
[68] D. B. Milosević, J. Phys. B **40**, 3367 (2007).
[69] V. Strelkov, Phys. Rev. Lett. **104**, 123901 (2010).
[70] L. Argenti and E. Lindroth, Phys. Rev. Lett. **105**, 053002 (2010).
[71] H. Wang, M. Chini, S. Chen, C.-H. Zhang, F. He, Y. Cheng, Y. Wu, U. Thumm, and Z. Chang, Phys. Rev. Lett. **105**, 143002 (2010).
[72] W.-C. Chu and C. D. Lin, Phys. Rev. A **82**, 053415 (2010).
[73] S. Gilbertson, H. Mashiko, C. Li, E. Moon, and Z. Chang, Appl. Phys. Lett. **93**, 111105 (2008).
[74] G. L. Kamta and A. F. Starace, Phys. Rev. Lett. **86**, 5687 (2001).
[75] G. L. Kamta and A. F. Starace, Phys. Rev. A **65**, 053418 (2002).
[76] J. M. Ngoko Djiokap, E. Foumouo, M. G. Kwato Njock, X. Urbain, and B. Piraux, Phys. Rev. A **81**, 042712 (2010).
[77] E. S. Toma, Ph. Antoine, A. de Bohan and H. G. Muller, J. Phys. B **32**, 5843 (1999).
[78] J. L. Krause, K. J. Schafer, and K. C. Kulander, Phys. Rev. Lett. **68**, 3535 (1992).
[79] G. W. F. Drake, in *Atomic, Molecular, and Optics Physics Handbook*, edited by G. W. F. Drake (AIP, New York, 1996), Chap. 11.
[80] Y. K. Ho, Phys. Rev. A **34**, 4402 (1986).
[81] E. Lindroth, Phys. Rev. A **49**, 4473 (1994).
[82] U. Fano, Phys. Rev. **124**, 1866 (1961).